J. Electroanal. Chem., 92 (1978) 45—53

ELECTROCHEMICAL KINETICS OF GOLD ELECTRODES IN SCN^-/DIMETHYLSULFOXIDE SOLUTIONS

M.E. MARTINS, C. CASTELLANO, A.J. CALANDRA and A.J. ARVÍA

Instituto de Investigaciones Fisicoquímicas Teóricas y Aplicadas, División Electroquímica, Sucursal 4, Casilla de Correo 16, 1900 La Plata (Argentina)

(Received 21st June 1977; in revised form 4th January 1978)

ABSTRACT

The electrochemical behaviour of the Au/SCN^- (DMSO) interface is studied at $25°C \leqslant T \leqslant 65°C$, by means of the triangular potential sweep technique and the RDE. Within a relatively limited potential range the main electrode process is:

$$3\ SCN^- = (SCN)_3^- + 2\ e$$

The kinetics of this reaction involves a mixed control. At higher potentials the electrodissolution of the base metal takes place. Side reactions occurring there make the overall process rather complex. The electrochemical behaviours of the Au/SCN^- (DMSO) and Au/SCN^- (ACN) are compared.

INTRODUCTION

The electrochemical oxidation of SCN^- ion dissolved as KSCN in different aprotic solvents [1—3] on Pt occurs within a potential range where the electrodissolution of the metal is practically negligible. Thus, the faradaic processes occurring at the Pt/KSCN (ACN) interface, for low SCN^- ion concentrations, $T < 10°C$ and in the presence of a supporting electrolyte, under a potentiodynamic perturbation [2] entails the formation of the $SCN^-/(SCN)_2$ redox couple. On the other hand, at high SCN^- ion concentrations and $T > 30°C$ [3], the overall reaction involves the formation of $(SCN)_x$-type polymers and decomposition products from $(SCN)_2$ as by-products. The course of these reactions, however, may be appreciably modified if the electrode material undergoes electrodissolution within the potential range of the SCN^- discharge. For this purpose it is interesting to investigate the electrochemical behaviour of the Au/KSCN (DMSO) interface.

Previous reports on the electrochemistry of different Au/electrolyte solution interfaces, such as Au/Cl^- (aq) [4], Au/SCN^- (aq) [5] and Au/KSCN (ACN) [6], indicate that the overall faradaic processes involve the electrodissolution of the metal yielding complex-ion species. This reaction depends on the solvent and on the halide or pseudo-halide ion present. This indicates that the competitive adsorption between anions and solvent molecules plays an important role in the kinetics of these reactions. A comparison between the behaviours of the Au/KSCN (DMSO) and Au/KSCN (ACN) interfaces offers therefore the possibility of looking with more detail into the degree of contribution of the adsorption

processes in the metal electrodissolution, taking into account that for a constant ionic strength DMSO acts as a stronger inhibitor than ACN [7,8].

EXPERIMENTAL

The experimental set-up is practically the same as described elsewhere [9,10]. The working electrodes are made from spectroscopic quality Au in the form of either different rotating Au discs (0.126 cm^2 and 0.071 cm^2) axially embedded in Teflon rods or Au wires (0.301 cm^2). The working electrode surface is mirror polished with fine alumina powder before running the measurements. The counter-electrode is a Pt sheet of large area. The electrode potentials are referred to the SCE.

Solutions of KSCN (c_0) + 0.5 M $KClO_4$ ($2.5 \times 10^{-3}\ M \leqslant c_0 \leqslant 10^{-2}\ M$) in carefully purified DMSO are employed under a nitrogen atmosphere. Experiments are performed at 25, 45 and 65°C, using single and repetitive triangular potential excursions initiated from cathodic to anodic potentials and the rotating disc electrode techniques, as reported elsewhere [9—11].

RESULTS

Rotating disc electrode E/I characteristics

Blank experiments at 25°C run between —0.6 V to 1.20 V at different potential sweep rates (v) exhibit a relatively small current contribution either anodic or cathodic, within the —0.3 V to 0.9 V range. When the solution contains KSCN the electrooxidation of SCN^- ion takes place at potentials between 0.1 V and 0.75 V without Au electrodissolution. The latter is observed when the anodic potential limit extends beyond 0.75 V. Regarding the first faradaic process the more reproducible results are those obtained from independent runs using a recently polished Au electrode and a fresh electrolyte solution.

The anodic E/I display obtained with the RDE at 2 mV s^{-1} exhibits a current plateau (I_L) (Fig. 1) which extends from 0.7 V to 0.9 V. Its height increases linearly both with $\omega^{1/2}$, the square root of the rotation speed and c_0. The corresponding half-wave potential ($E^a_{1/2}$) increases linearly with log ω. For $c_0 = 5 \times 10^{-3}\ M$ at 1410 rpm the $E^a_{1/2}$ are 0.720 ± 0.005 V at 24.5°C and 0.631 ± 0.025 V at 45.1°C.

The portion of the anodic E/I profile extending up to (0.6 I_L), fits a linear E/log I relationship with a slope close to the 2.3 ($2\ RT/F$) ratio. The open circuit potential after anodizing exhibits the characteristics of a reversible rest potential. For $c_0 = 5 \times 10^{-3}\ M$ the apparent exchange current density (i_0^{app}) extrapolated at the rest potential lies between 3.6×10^{-8} A cm^{-2} and 6.3×10^{-8} A cm^{-2} at 24.4°C and between 4.1×10^{-7} A cm^{-2} and 4.3×10^{-7} A cm^{-2} at 45.0°C.

Voltammetric runs in the —0.3 V to 0.75 V range with fresh electrolyte solution

Single symmetric triangular potential sweep voltammograms (Fig. 2) run at different temperatures in the —0.3 V to 0.75 V range show a well defined anodic

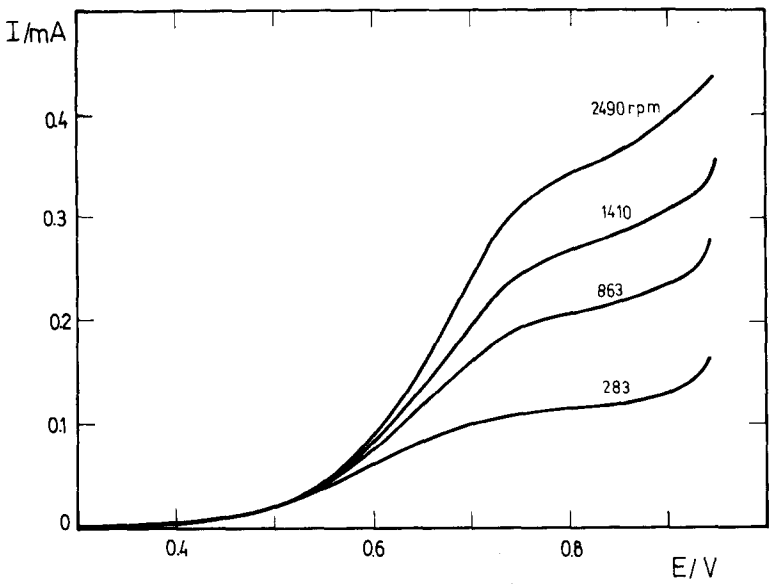

Fig. 1. Current/potential curves run at 2 mV s^{-1} with the RDE at different rotation speeds. $c_0 = 10^{-2}$ *M*, 45°C, 0.071 cm^2.

current peak (I_{ap}) during the forward excursion and a broader cathodic current peak (I_{cp}) during the returning scan. The former is preceded by a small current plateau extending from −0.05 V to 0.3 V. This prewave which is only noticed under potentiodynamic conditions involves a charge of ca. 10 mC cm^{-2} which is independent either of v, c_0 or T. Its height, however, increases linearly with v. The prewave is always present in the blanks independently of the degree of purification reached for the solvent-supporting electrolyte system.

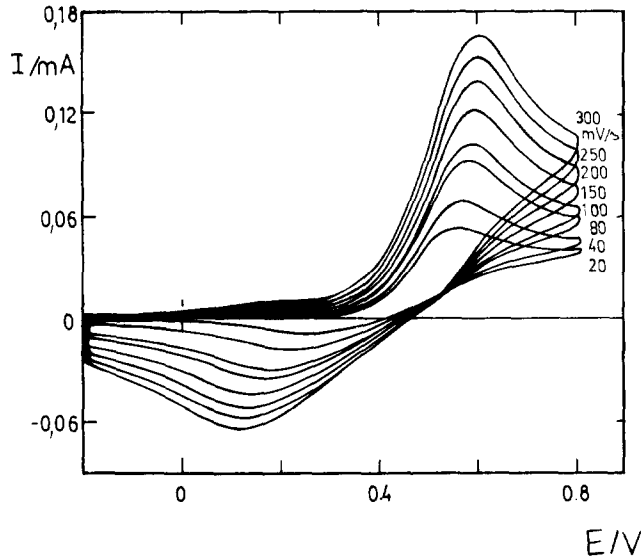

Fig. 2. *E/I* voltammograms run with single triangular potential sweeps at different v. $c_0 = 2.8 \times 10^{-3}$ *M*, 45.1°C, 0.301 cm^2.

Both I_{ap} and I_{cp} increase linearly with $v^{1/2}$ and at a constant v, the former increases linearly with c_0. Both E_{ap} and E_{cp} depend linearly on log v, the slopes of the straight lines being equal to the ratio $2.3(RT/F)$ for the anodic reaction and to the ratio $2.3(2\,RT/F)$ for the cathodic reaction. The difference between E_{ap}, the anodic current peak potential, and E_{cp}, the cathodic current peak potential, increases with v. Linear E_{ap} vs. log I_{ap} and E_{cp} vs. log I_{cp} plots have also been obtained. The slope of the former is close to the ratio $2.3(2\,RT/F)$ while that of the latter approaches the ratio $2.3(4\,RT/F)$.

Temperature dependences

The range of the electrochemical reactions becomes smaller as the temperature (T) increases and the ($E_{ap} - E_{cp}$) difference diminishes accordingly. The I_{cp}/I_{ap} ratio as determined in the usual way is slightly lower than one, but approaches this figure as T increases. The different kinetic parameters fit Arrhenius-type equations reasonably well. The different apparent activation energies (ΔH^*) are assembled in Table 1.

E/I displays under repetitive potential scanning. Influence of anodization

The repetitive triangular potential scans between −0.2 V and 0.55 V (Fig. 3) show an activation of both the anodic and the cathodic processes during cycling with the simultaneous decrease of I_{ap} and increase of I_{ac} as n, the number of scans, increases. After $n \approx 20$ a stationary E/I profile is obtained.

Runs between −0.42 V and 0.55 V with an anodization time τ, ($30\ s \leqslant \tau \leqslant 15$ min) at 0.55 V between the anodic and the cathodic potential excursions (Fig. 4) show that at least two products are formed within the anodic potentials swept, as is revealed by the cathodic E/I profile. As τ increases the cathodic current contribution at the anodic extreme becomes constant while I_{cp} shifts towards more cathodic potentials. The same results are obtained from those runs where I_{ap} has been fully developed prior to the anodization.

Influence of the anodic and cathodic potential limits on the E/I displays

When the anodic potential limit exceeds 0.75 V the anodic current increases quite remarkably because of both the electrodissolution of Au and the electro-

TABLE 1

Experimental activation energies

Magnitude	ΔH^*/kcal mol^{-1}
Anodic limiting current	2.96 ± 0.15
Anodic current peak	1.64 ± 0.15
Diffusion coefficient	3.25 ± 0.20
Kinematic viscosity	3.85 ± 0.10
Anodic limiting current (calculated)	2.81 ± 0.20
Anodic current peak (calculated)	1.63 ± 0.10

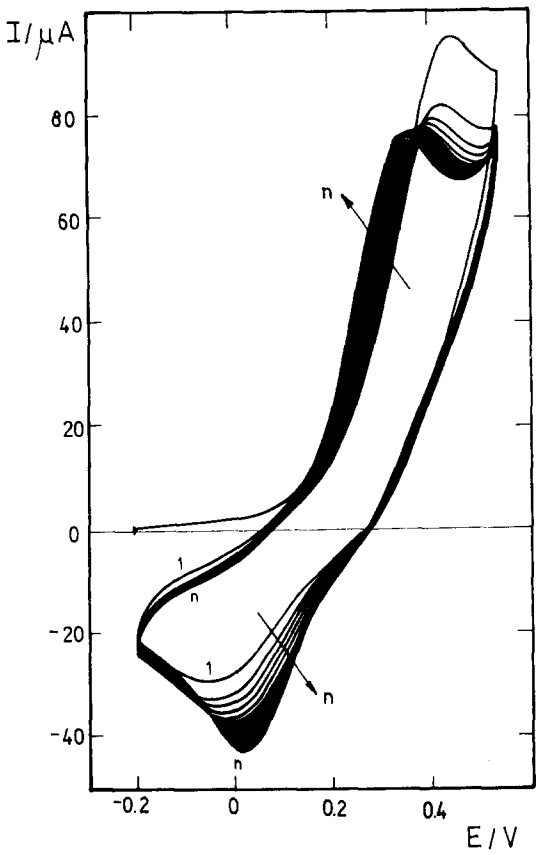

Fig. 3. *E/I* voltammograms run at 50 mV s^{-1} with repetitive triangular potential sweeps. c_0 = 2.8 x 10^{-3} *M*, 25.0°C, 0.301 cm^2.

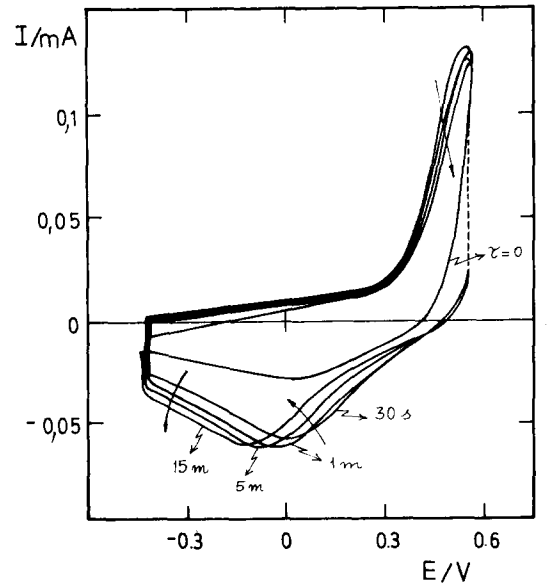

Fig. 4. *E/I* voltammograms run with single triangular potential sweeps at 50 mV s^{-1} with different interruption times (τ) at the anodic potential limit. c_0 = 2.8 x 10^{-3} *M*, 25.0°C, 0.301 cm^2.

decomposition of the solvent-supporting electrolyte system (Fig. 5). The electroreduction of the soluble Au species yielded by the anodic reaction is related to the small cathodic current peak located at ca. 0.85 V. The current efficiency for Au electrodissolution at this potential as Au(III) exceeds 100% and calculated as Au(I) is about 70%. It is likely that the dissolution takes place predominantly as Au(I), the latter participating in Au(I)/Au(III)/Au equilibria probably in the same way as already known for other similar systems [4—6]. The rest of charge is entailed in the electrooxidation of the solvent.

When the cathodic potential limit is increased from —0.4 to —0.7 V the cathodic decomposition of the solvent yields products which are related to spurious anodic and cathodic current peaks appearing in the 0.3 V to —0.9 V range. The impurity accumulation produces a drastic change of the potentiodynamic *E/I* profiles. Then, the voltammograms contain lower anodic and cathodic current peaks both spread in broader potential ranges.

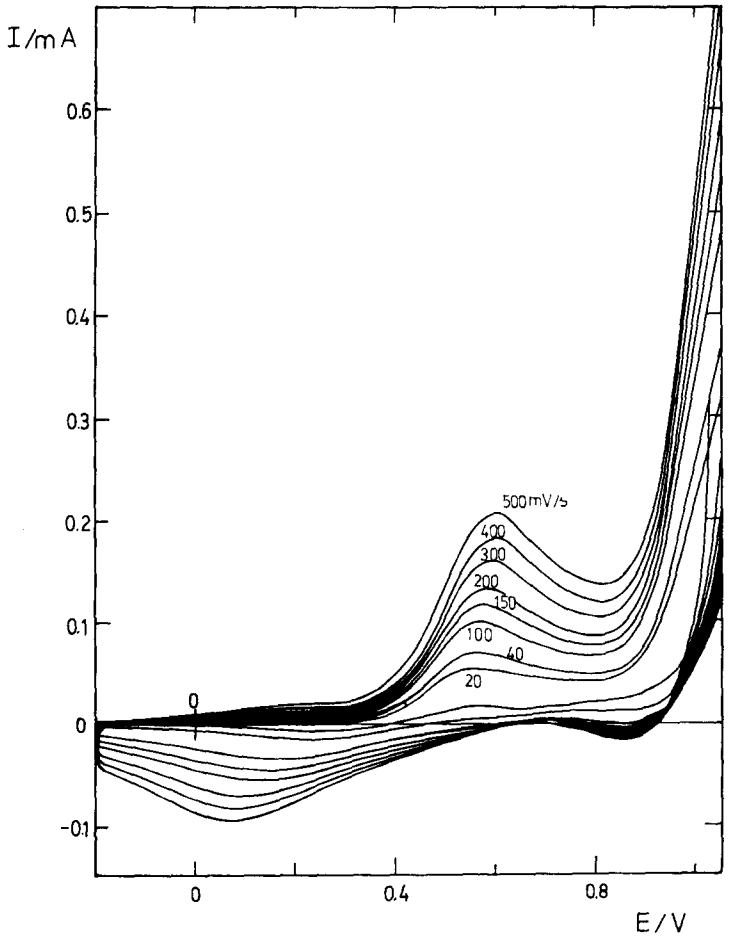

Fig. 5. *E/I* voltammograms run with single triangular potential sweeps at different *v*. c_0 = 2.8×10^{-3} *M*, 45.1°C, 0.301 cm^2.

DISCUSSION

The electrochemical behaviour of the Au/SCN^- (DMSO) interface in the −0.2 V to 0.8 V potential range as deduced from the potentiodynamic response of the system is apparently more complex than that previously reported for the Au/SCN^- (ACN) interface [6]. Thus, in the former system the electrodissolution of the metal takes place at more anodic potentials than in the latter and it is preceded by the SCN^- ion electro-oxidation. The different responses of those systems are related on one side to the smaller electrochemical stability potential range of DMSO as compared to that of ACN [12] and to the inhibiting influence of DMSO on metal electrodissolution processes [7,8].

When the potential perturbation is constrained between −0.2 and 0.8 V, the main process corresponds to the electro-oxidation of SCN^- ion according to the following reaction:

$$3\ SCN^- = (SCN)_3^- + 2\,e \qquad (1)$$

The reverse reaction corresponds to the cathodic process. Reaction (1) corresponds to the type of process already described for various electrochemical interfaces related to the $X_2/X_3^-/X^-$ system, where X stands for the halide or pseudohalide species [13–17].

The anodic reaction, however, is preceded by a small limiting current which extends from ca. 0.1 to ca. 0.3 V. Its electrochemical characteristics and charge magnitude reveal that during the anodic potential sweep the first process involves the formation of a surface film on the electrode, which may be due either to the electrosorption or electrodecomposition of the solvent on the clean metal surface or to an equivalent reaction due to some undetermined impurity trace. In any case, the interesting point is that the discharge of SCN^- ion takes place not on a bare metal but on a film covered gold electrode. The film formation, on the other hand, impedes the metal electrodissolution at lower anodic potentials. Under these circumstances, the electrooxidation of SCN^- ion occurs on an apparently inert electrode so that when the corresponding potentiodynamic *E/I* profile is corrected for the preceding wave the resulting shape fits the equation derived for an irreversible reaction under diffusion control [18].

The diffusion coefficient (Table 3) of the reacting species can be calculated. For this purpose the αn_a product (Table 2) is obtained from the relationship:

$$E_{ap} = E^a_{1/2} - 1.857\,(RT/\alpha n_a F) \qquad (2)$$

If α, the transfer coefficient, is taken as 0.5, n_a, the number of electrons playing part in the r.d.s. of the electrooxidation reaction, should be one. With those figures together with n, the number of electrons per reacting ion equal to 2/3, D, the diffusion coefficients derived from the potentiodynamic displays and from the RDE data using Levich's equation [19] come out in good agreement and they compare well with those given in the literature [3,4,6]. The temperature dependences of I_L, D, ν and I_{ap} fit the characteristics of an electrochemical reaction which is largely diffusion controlled.

When the potential sweep extends to the region where the electrooxidation of the solvent occurs, the *E/I* profile related to reaction (1) changes quite markedly. These changes are also assisted by the presence of traces of water, which

TABLE 2

Values of αn_a derived from E/I voltammograms for $2 \leqslant v \leqslant 0.45$ V s^{-1}

$10^3 \times c_0/M$	T/°C	$(\alpha n_a)_{av}$
5.0	24.4	0.43
5.0	45.2	0.47
5.0	64.8	0.40
2.5	24.6	0.47
2.5	45.0	0.48
2.5	64.0	0.53
1.0	45.0	0.41

TABLE 3

Diffusion coefficient of SCN^- ion

T/°C	$10^6 \times D$/cm^2 s^{-1}
24.5 ± 0.1	1.15 ± 0.01
45.1 ± 0.1	1.60 ± 0.01
64.4 ± 0.1	2.23 ± 0.01

reacts electrochemically yielding dimethylsulphone and H^+ ions [20,21]. The H^+ ion formation is voltammetrically detected as a current peak at −0.95 V. At higher cathodic potentials the DMSO electroreduction yields different sulphide-type species [23]. The formation of these by-products alters the electrochemical interface and modifies the E/I characteristics and, consequently, the kinetic parameters which are derived from them.

The electrodissolution of Au only occurs in the anodic potential range where other reactions are simultaneously produced. But independently of this the dissolved metal can be cathodically reduced at ca. 0.85 V, the corresponding cathodic current depending on the concentration of soluble Au. Therefore, the inhibiting influence of DMSO in the electrodissolution of Au is similar as for other metals previously investigated.

ACKNOWLEDGEMENT

INIFTA is sponsored by the following institutions: Universidad Nacional de La Plata, Consejo Nacional de Investigaciones Científicas y Técnicas (Argentina) and Comisión de Investigaciones Científicas (Pcia. de Buenos Aires).

REFERENCES

1 G. Cauquis and G. Pierre, C.R. Acad. Sci. (Paris), Série C, 226 (1968) 883; G. Cauquis and G. Pierre, Bull. Soc. Chim. Fr., 6 (1972) 2244.
2 R. Pereiro, A.J. Arvia and A.J. Calandra, Electrochim. Acta, 17 (1972) 1723.
3 C. Martínez, A.J. Calandra and A.J. Arvia, Electrochim. Acta, 17 (1972) 2153.
4 J. Herrera Gallego, C.E. Castellano, A.J. Calandra and A.J. Arvia, J. Electroanal. Chem., 66 (1975) 207.
5 J.N. Gaur and G.M. Schmid, J. Electroanal. Chem., 24 (1970) 279.

6 M.E. Martins, C.E. Castellano, A.J. Calandra and A.J. Arvia, J. Electroanal. Chem., 81 (1977) 291.
7 S. Thibault and J. Talbot, 3rd European Symp. on Corrosion Inhibitors, Ferrara, 1970.
8 D. Posadas, A.J. Arvia and J.J. Podestá, Electrochim. Acta, 16 (1971) 1041.
9 J. Wargon and A.J. Arvia, Electrochim. Acta, 16 (1971) 1619.
10 M.E. Martins, G. Paús, A.J. Calandra and A.J. Arvia, Anales Asoc. Quim. Arg., 57 (1969) 91.
11 G. Paús, A.J. Calandra and A.J. Arvia, Anales Soc. Cient. Arg., 192 (1971) 35.
12 A.K. Covington and T. Dickinson, Physical Chemistry of Organic Solvents Systems, Plenum Press, New York, 1974.
13 M.C. Giordano, J.C. Bazán and A.J. Arvia, Electrochim. Acta, 11 (1966) 1553.
14 A.J. Arvia, M.C. Giordano and J.J. Podestá, Electrochim. Acta, 14 (1969) 389.
15 V.A. Macagno, M.C. Giordano and A.J. Arvia, Electrochim. Acta, 14 (1969) 335.
16 L. Sereno, V.A. Macagno and M.C. Giordano, Electrochim. Acta, 17 (1972) 561.
17 G. Cauquis and G. Pierre, C.R. Acad. Sci. (Paris), Série C, 269 (1969) 740.
18 R. Nicholson and I. Shain, Anal. Chem., 36 (1974) 706.
19 V.G. Levich, Physicochemical Hydrodynamics, Prentice Hall, Englewood Cliffs, 1962.
20 H.E. Zittel and F.J. Miller, Anal. Chim. Acta, 37 (1967) 741.
21 J. Herrera Gallego, M.E. Martins, A.J. Calandra and A.J. Arvia, in preparation.
22 C. Martínez, A.J. Calandra and A.J. Arvia, Anales Asoc. Quim. Arg., 60 (1972) 413.
23 T.C. Franklin and H. Kagawa, Electrochim. Acta, 17 (1972) 1213.